Advanced Steel Construction – Vol. 19 No. 4 (2023) 389–402
DOI:10.18057/IJASC.2023.19.4.8

DEEP LEARNING DAMAGE IDENTIFICATION METHOD FOR STEEL-FRAME BRACING STRUCTURES USING TIME–FREQUENCY ANALYSIS AND CONVOLUTIONAL NEURAL NETWORKS

Xiao-Jian Han [1], Qi-Bin Cheng [1] and Ling-Kun Chen [2, 3, 4, *]

[1] *College of Civil Engineering, Nanjing Tech University, Nanjing, 211800 Jiangsu, China*
[2] *College of Civil Science and Engineering, Yangzhou University, Yangzhou, 225127 Jiangsu, China*
[3] *Department of Civil and Environmental Engineering, University of California, Los Angeles, CA 90095 USA*
[4] *School of Civil Engineering, Southwest Jiaotong University, Chengdu, 610031 Sichuan, China*
** (Corresponding author: E-mail: lingkunchen08@hotmail.com)*

ABSTRACT

Lattice bracing, commonly used in steel construction systems, is vulnerable to damage and failure when subjected to horizontal seismic pressure. To identify damage, manual examination is the conventional method applied. However, this approach is time-consuming and typically unable to detect damage in its early stage. Determining the exact location of damage has been problematic for researchers. Nevertheless, detecting the failure of lateral supports in various parts of a structure using time–frequency analysis and deep learning methods, such as convolutional neural networks, is possible. Then, the damaged structure can be rapidly rebuilt to ensure safety. Experiments are conducted to determine the vibration acceleration modes of a four-storey steel structure considering various support structure damage scenarios. The acceleration signals at each measurement point are then analysed with respect to time and frequency to generate appropriate three-dimensional spectral matrices. In this study, the MobileNetV2 deep learning model was trained on a labelled picture collection of damaged matrix images. Hyperparameter tweaking and training resulted in a prediction accuracy of 97.37% for the complete dataset and 99.30% and 96.23% for the training and testing sets, respectively. The findings indicate that a combination of time–frequency analysis and deep learning methods may pinpoint the position of the damaged steel frame support components more accurately.

ARTICLE HISTORY

Received: 18 July 2022
Revised: 15 June 2023
Accepted: 27 August 2023

KEYWORDS

Damage identification;
Bracing system;
Deep learning;
Convolutional neural networks (CNNs);
Time–frequency analysis;
MobileNetV2

1. Introduction

A support system is an important part of a steel structure. It ensures that the entire steel structure and individual components have sufficient stability and stiffness. Moreover, the system enables the transfer of horizontal forces and absorption of seismic energy as well as improves the overall performance of the steel structure. Among all types of supports, supports between two adjacent columns are vital for ensuring overall stability, horizontal load transfer, and earthquake resistance. Cross-diagonal bracing, splay diagonal bracing, and door-type support are typically adopted as column supports. Because the stiffness of the column support system must be consistent, steel angles or channels are typically used.

However, owing to the inherent defects of steel materials, environmental corrosion, natural disasters, and other factors, the inter-column support system in a steel may be damaged during use. With the accumulation of damage, the failure of the support, particularly under the action of a seismic load, may lead to the inability of the structure to transfer horizontal load effectively, resulting in significant deformation, structural instability, or collapse.

For a given steel structure, the damage identification method typically involves several steps, such as locating the damage, identifying the type and degree of damage, and estimating the remaining life of the structure. The current damage detection methods are primarily manual visual observation or the use of special detection equipment. Generally, the bolts in steel structures have been found to be loose, rusted, broken, or sustaining other types of damage.

With the application of various structural health monitoring (SHM) systems, the number of sensors used to obtain the state data of a structure for evaluating the health status continues to increase. These sensors provide supporting data for the subsequent design of structural reinforcement and maintenance scheme [1–5]. Therefore, analysing the location and degree of damage of structural support systems using the dynamic response data of structures obtained by an SHM system or detection instrument is advantageous.

Structural damage identification methods are typically designed considering three aspects: (a) optimisation of modal structural parameters to identify indicators susceptible to structural damage; (b) use of an artificial intelligence algorithm to determine the location and degree of damage; and (c) structural damage identification using the combination of structural dynamics, finite element (FE) modelling, vibration tests, and artificial intelligence algorithms. Yazdanpanah et al. [6–7] employed incremental non-linear dynamic analysis to diagnose damage to steel moment-resisting frames in different seismic scenarios. Tam et al. [8] used noise, incomplete modal data, and a depth feedforward neural network to locate and quantify damage in truss structures. Xin et al. [9] proposed an effective method for detecting non-linear structural degradation based on variational modal decomposition. Liu et al. [10] analysed the sensitivity of structural modal parameters to damage and quantified the degree of reduction in structural stiffness. Han et al. [11] proposed a method based on the Hilbert–Huang transform to identify structural modal parameters and diagnose structural damage. Paral et al. [12] analysed the overall vibration signal using a wavelet transform and convolutional neural network (CNN) to identify the damage to the local connection of a two-storey structural steel frame. Pathirage et al. [13–14] developed a deep learning framework for a sparse automatic encoder for structural damage identification. Hakim et al. [15–16] used an integrated neural network to locate and evaluate damage to an I-steel structure. Seventekidis et al. [17] used the data samples of an optimised FE model as input into a CNN for structural damage identification. Liu et al. [18] created a large-scale dataset based on a structural transfer function and established a new framework for structural damage identification using a one-dimensional CNN. Figueiredo et al. [19] combined the SHM field data and FE modelling data of a bridge structure to form a machine learning model input for bridge damage assessment.

Nadith et al. [20] developed an autoencoder-based deep neural network capable of analysing the link between structural vibrations and structural damage, laying the groundwork for diagnosing non-linear structural damage. Gordan et al. [21] used the vibration testing of a plate and beam bridge model to extract the top four orders of their inherent frequencies as input vectors for support vector machines, neural networks, and classification regression trees. Their findings indicated that the procedure was entirely accurate. Ali and Cha [22] suggested a technique based on deep learning for identifying subsurface damage to steel members in steel truss bridges; the field test results on a steel bridge demonstrated the high accuracy and practicality of the approach. Kourehli and Ghadimi [23] used the emergency learning algorithm of an inline sequential limit learning machine to anticipate the fracture depth and position of a Timoshenko beam. Teng et al. [24] used FE numerical analysis and experimental data to provide a considerable amount of damage data for a CNN. This improved the CNN-based damage detection algorithms in engineering practice.

Typically, lateral bracing is used to ensure the overall rigidity of a steel structural system; however, it is prone to damage and failure when the structure is subjected to horizontal seismic loads. A typical approach to determine damage is manual examination; however, this requires a considerable amount of time, and some damage points may not be detected. This problem has long been a

source of contention among academics attempting to identify the exact location of damage. The time–frequency domain and CNNs have been used to identify lateral bracing failure in various parts of a structure. Then, the damaged part of the structure is located and repaired to ensure structural safety.

In this study, modal information is obtained from structural detection. The spectrum of structural time–frequency domain analysis is obtained to establish a labelled spectrum sample library. The spectrum is classified through an image recognition method based on a CNN; MobileNetV2 derives the classification model. In subsequent stages, the spectrum analysis diagram can be inputted into the model to determine the damage location. Limited research has been conducted on damage identification methods combining signal analysis and image processing. This method is explored in this study, and satisfactory results are obtained.

The remainder of this paper is organised as follows. The details of the steel frame vibration testing procedure covering the test object, design, instruments, outcome analysis are presented in Section 2. The construction and results of the FE modelling process for the steel frame structure are discussed in Section 3. The characteristics, construction, and performance evaluation of the MobileNetV2 model for structural damage identification are presented in Section 4. Finally, the conclusions drawn based on the MobileNetV2 classification performance and vibration testing results are summarised in Section 5.

2. Vibration testing of steel frame model

2.1. Steel frame model description

A four-storey steel frame model is used in this study. Because this model was evaluated on a seismic simulation shaker with associated equipment and structure, it was designed with a geometric similarity ratio of 1:10. The model height, span spacing, floor height, beam length are 1.8, 0.6, 0.45, and 0.56 m, respectively. For the beam and inter-column support sections, 60 × 30 × 2.5-mm cold-formed thin-walled channels are used. According to the dynamic similarity ratio theory, the model weighs 45.1 kg, and the counterweight is 155 kg. The fundamental frequency of the structure is 5.165 Hz.

The parameters of the steel frame members are listed in Table 1. A steel frame without a bracing system is illustrated in Fig. 1.

Fig. 1 Steel frame model without bracing system (left) and with bracing member (right)

Table 1
Parameters of members of steel frame model

Parameters		
Height (mm)		1800
Quality (kg)		45.1
Counterweight (kg)		766.20
Column	Column height (mm)	450
	Section size (mm)	40×40×2
	Area (mm^2)	287
	Moment of inertia (mm^4)	66600
	Moment of area (mm^3)	3330
Beam	Beam length (mm)	560
	Section size (mm)	60×30×2.5
	Area (mm^2)	240
	Moment of inertia (mm^4)	143800
	Moment of area (mm^3)	4890

2.2. Test scheme design

Eight bracing members were placed on both sides of each of the four layers of the steel frame model. The spatial layout and serial numbers of members are shown in Fig. 2. The serial numbers facilitate the construction of the deep learning model and image dataset as well as associated labels.

Five dismantling conditions were set for the bracing members in the vibration test. Under the first condition, no dismantling of the bracing members was set. The second condition requires the dismantling of the bracing element. Two, three, and four bracing members are removed for the third, fourth, and fifth types of structures, respectively. A total of 69 dismantling conditions are listed in Table 2, and vibration tests are conducted under these conditions. When three or four members are dismantled, note that not all potential combinations are listed in the table.

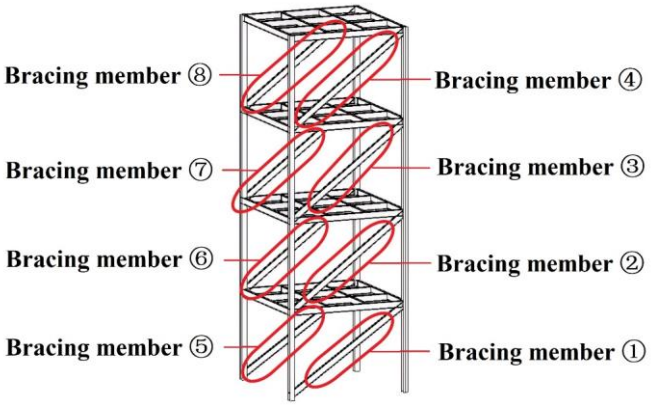

Fig. 2 Spatial layout and serial numbers of eight bracing members

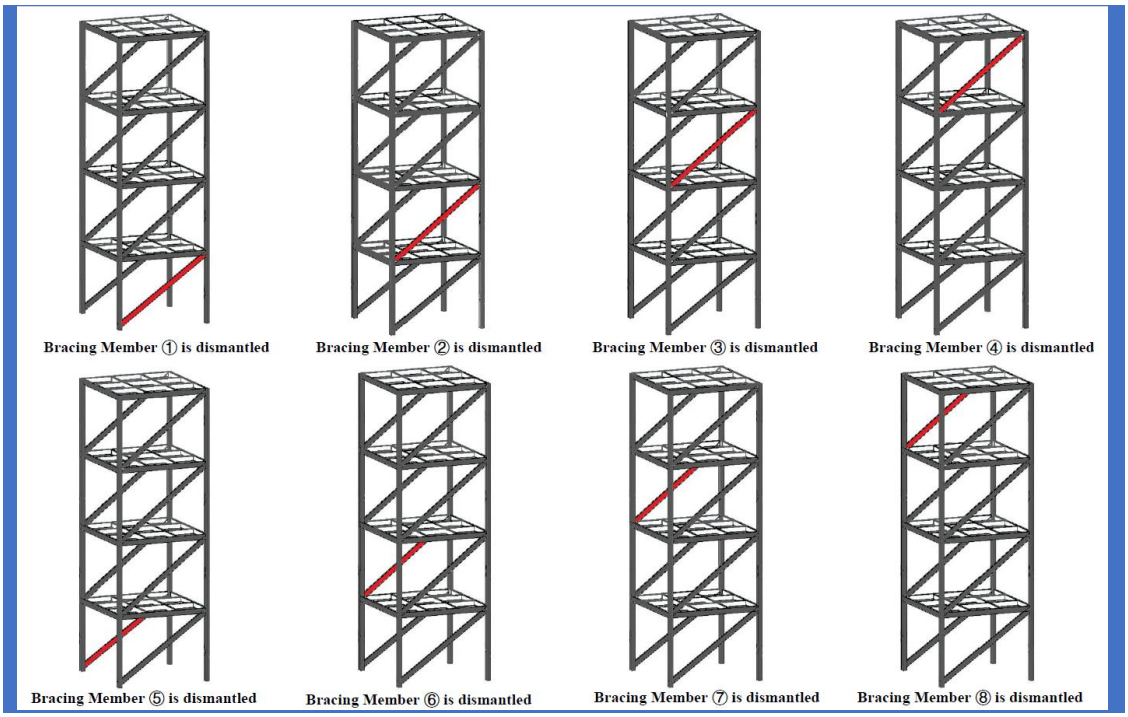

Fig. 3 Schematic of dismantling working condition of bracing member

Under each dismantling condition, a displacement load of 1 cm is applied to the top layer of the steel frame. Then, the resulting acceleration signals of each layer are acquired during the natural vibration stage. The vibration direction of the steel frame is shown in Fig. 4, and the spatial layout of the acceleration measurement points is shown in Fig. 5.

The selection of the appropriate sampling frequency of structural vibration signals is crucial. The use of a low sampling frequency results in signals with limited information content, whereas the use of a high sampling frequency leads to low-frequency resolution. Hence, the sampling frequency must satisfy or slightly exceed the Nyquist sampling frequency [25–28]. Specifically, to retain the information content of continuous signals in the sampled signal to the extent possible, the sampling frequency used is generally 2.56–4 times the highest frequency of the constant signal.

The preliminary results of the FE simulations indicate that the first-order and fourth-order frequency ranges of the steel frame are 5.7–6.5 and 30–31 Hz, respectively. A sampling frequency of 128 Hz was selected, and the signal acquisition time was set to 10 s. To reduce the test error, the acquisition of acceleration signals was repeated three times under each working condition.

Fig. 4 Vibration direction of steel frame

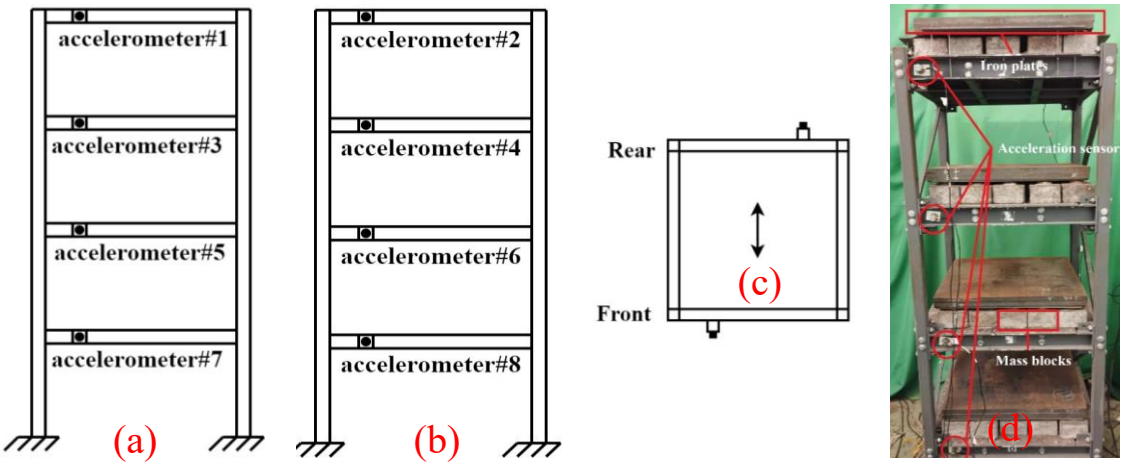

Fig. 5 Arrangement of acceleration measurement points: (a) front view, (b) rear view, (c) top view, and (d) sensor arrangement

2.3. Test instruments

A vibration test was conducted using an NI9234 signal acquisition device with an LC0108 IEPE acceleration sensor as well as the DASP acquisition and processing software. The sensor and acquisition equipment are shown in Fig. 6. This type of acceleration sensor fits the criteria of this test owing to its light weight, high sensitivity, and wide frequency range. The sensors were calibrated to obtain accurate and reliable data. The performance parameters of the acceleration sensors are listed in Table 2. A magnetic base was attached to the acceleration sensor at the steel measuring site. The acquisition software includes tools for signal and modal analyses. The acquisition frequency employed in the test was 120 Hz, and the sampling frequency was determined using the maximum value of FFT × 2.

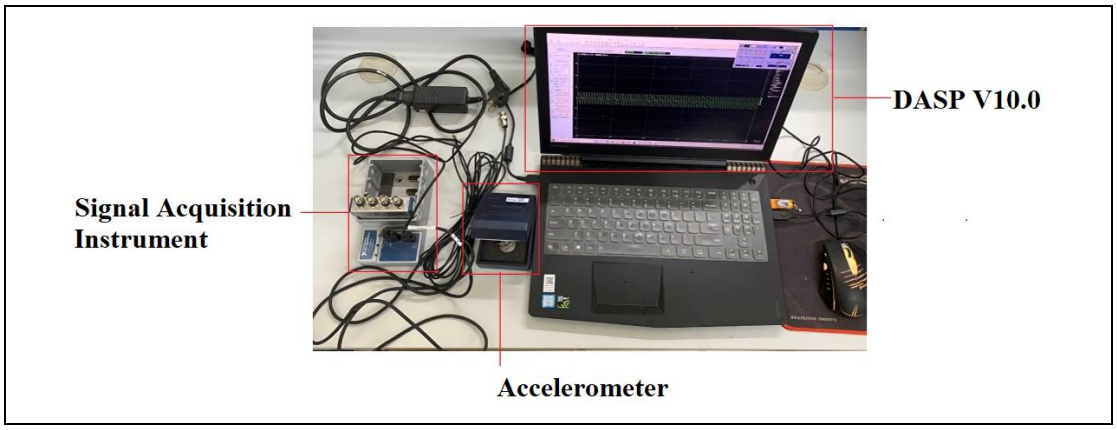

Fig. 6 Test instrument

Table 2
Performance parameters of LC0108 acceleration sensors

Frequency range (Hz)	Sensitivity (Mv/EU)	Weight (mg)	Thread Specification	Boundary Dimension
0.35-5000	497-504	17	M5	Hexagon Side length: 14mm Height: 20mm

2.4. Analysis of vibration test results

Fourier transform can be used to analyse the frequency content of non-stationary signals; its computational algorithms demonstrate high precision and efficiency. This transform converts the time-domain acceleration signals into frequency-domain signals. The forward and inverse discrete-time Fourier transforms for the discrete-time signal, $X[n]$, are determined using Equations (1) and (2), where N is the number of signal samples:

$$X\left(e^{j\omega}\right)=\sum_{n=\langle N\rangle}X[n]e^{-j\omega n} \tag{1}$$

$$X[n]=\frac{1}{2\pi}\int_{2\pi}X\left(e^{j\omega}\right)e^{j\omega n}d\omega \tag{2}$$

The discrete-time Fourier transform analyses the acquired acceleration signals using 1024 signal samples. The time-domain acceleration signals are converted into frequency-domain signals, and the natural vibration frequencies of the steel frame are extracted. Under each operating condition, the average frequency is computed over three test repetitions and used as the final frequency result.

To account for the influence of torsion, each layer has two diagonally arranged accelerometers. The overlaid time-domain signals acquired by the accelerometers can be used to calculate both advection and torsion components; however, only the advection component is utilised in this study. The time-domain and frequency-domain analysis results for the top layer are presented in Figs. 7 and 11, respectively. In Figs. 9 and 10, the time-domain plots depict the two acceleration averages of the top layer. The frequency-domain plots show the torsional components at 5.25 (Fig. 9) and 5.125 Hz (Fig. 10).

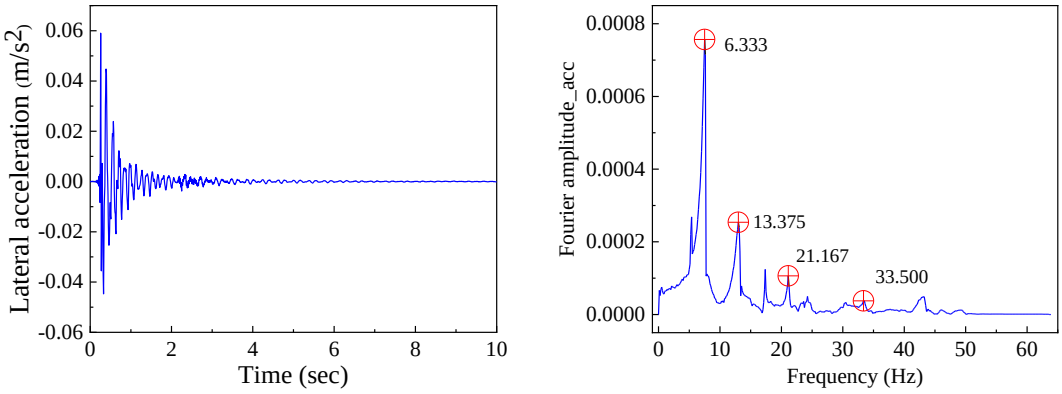

(a) Time-domain signal (b) Frequency-domain signal

Fig. 7 Time-domain and frequency domain curves when no support member is removed

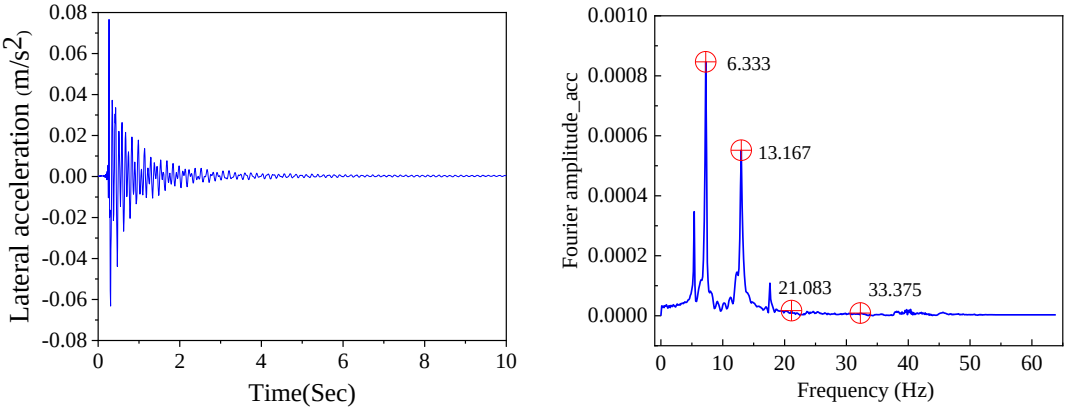

(a) Time-domain signal (b) Frequency-domain signal

Fig. 8 Time-domain and frequency-domain curves of one support member removed (#1)

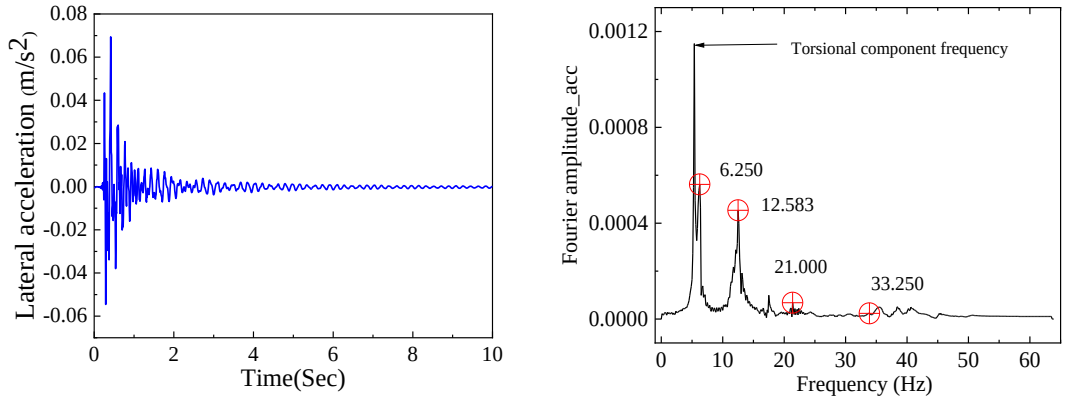

(a) Time-domain signal (b) Frequency-domain signal

Fig. 9 Time-domain and frequency-domain plots for two support members removed (#12)

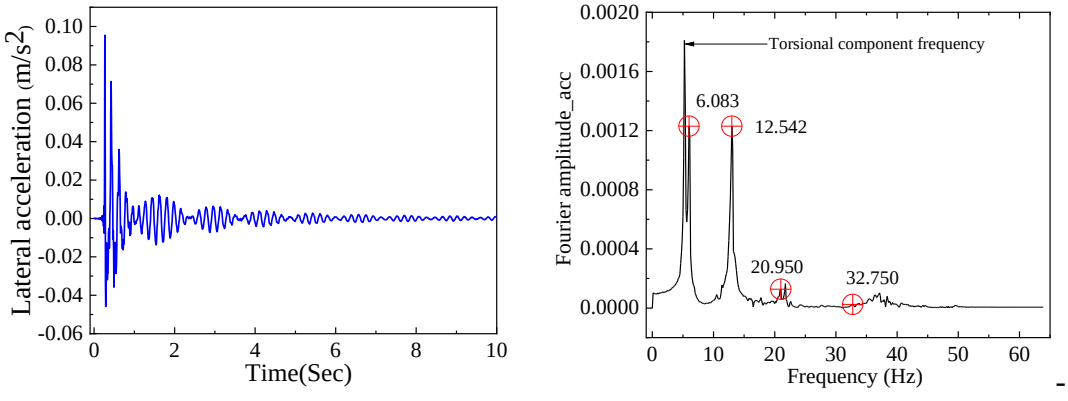

(a) Time-domain signal (b) Frequency-domain signal

Fig. 10 Time-domain and frequency-domain diagrams of three support members removed (#123)

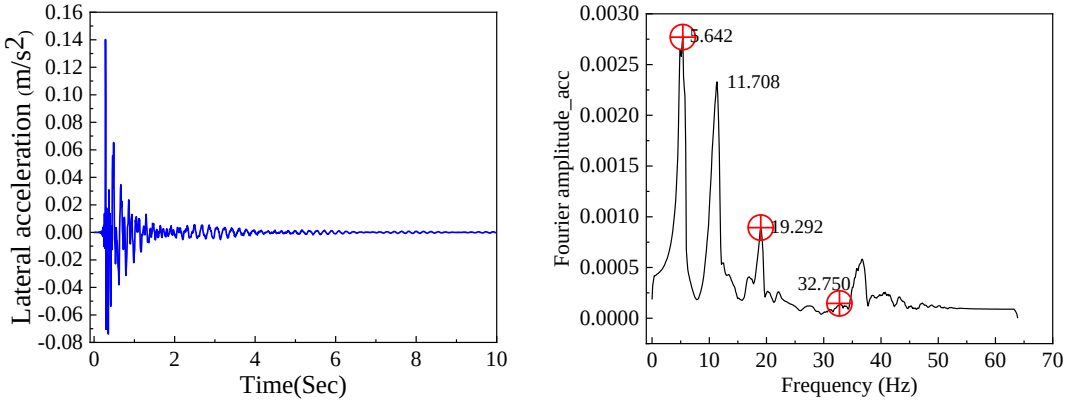

(a) Time-domain signal (b) Frequency-domain signal

Fig. 11 Time-domain and frequency-domain diagrams of four support members removed (#1234)

Table 3
First-order to fourth-order steel frame frequencies under some working conditions

Working Condition	The frequencies/Hz			
	1st order	2nd order	3rd order	4th order
Undamaged	6.333	13.375	21.167	33.500
#1	6.333	13.167	21.083	33.375
#12	6.250	12.583	21.000	33.250
#123	6.083	12.542	20.950	32.750
#1234	5.642	11.708	19.292	32.750

The maximum energy signal increases with the frequency-domain peak amplitude. By combining the spectral signals with preliminary FE analysis results, the first-order up to the fourth-order steel frame frequencies can be obtained. The frequencies under some working conditions are listed in Table 3.

The wavelet transform was used to analyse the acceleration signals in the time-frequency domain; the corresponding three-dimensional spectral matrices were obtained. Examples of these matrices under certain operating conditions are shown in Fig. 12. The horizontal and vertical axes correspond to frequency and time values, respectively. Colours are used to code the scale of acceleration values at specific time-frequency points.

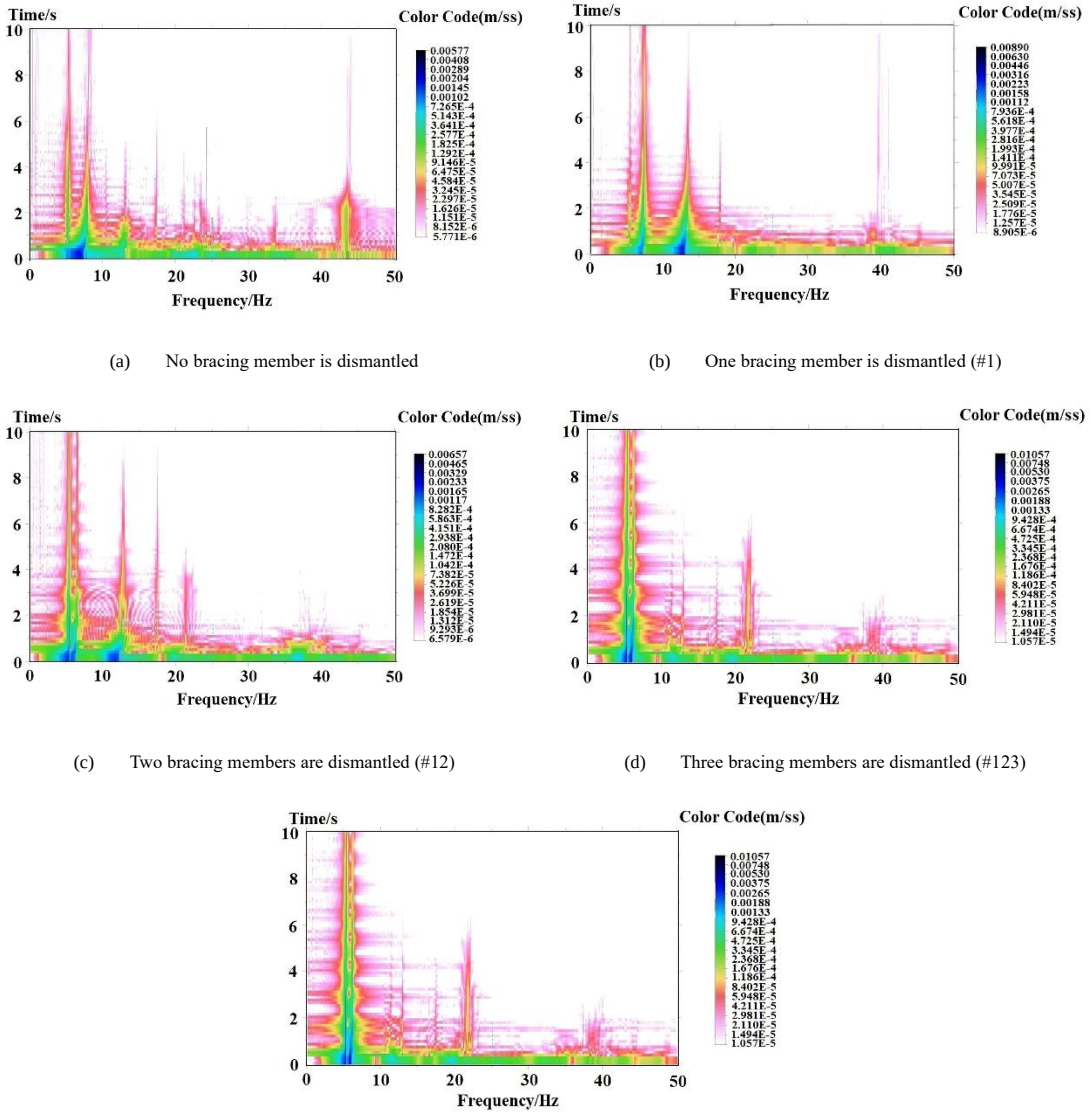

(a) No bracing member is dismantled

(b) One bracing member is dismantled (#1)

(c) Two bracing members are dismantled (#12)

(d) Three bracing members are dismantled (#123)

(e) Four bracing members are dismantled (#1234)

Fig. 12 Three-dimensional time-frequency matrices of acceleration signals under some working conditions

Each three-dimensional spectral matrix contains joint time–frequency information, which can characterise structural damage more accurately than time-domain or frequency-domain representation. Additionally, the proposed time–frequency representations are more sensitive to the dismantling of the bracing members of the steel frame model.

3. Numerical simulation of steel frame model

3.1. FE modelling

FE modelling and analysis of the steel frame were performed using the ABAQUS software. The FE model was modified according to the frequencies obtained from the vibration tests to maintain the error within an acceptable range. The steel frame was geometrically modelled as a rod-like system structure. Some of the geometric modelling details are as follows. First, the node coordinates are specified according to the geometric dimensions of the steel

frame. Additionally, line units are created using a node-to-node correspondence method where all nodes are rigidly set, and the bottom of columns is fully fixed. Datum planes and reference points are established to divide the steel frame and generate floor slabs and frame beams. The frame beams must be longitudinal to form common coupling nodes with the floor slabs.

The unit system, material properties, and section properties are set during modelling. The unit system is set as follows: length, force, and stress are measured in meter, newton, and pascal, respectively. The characteristics of steel and iron materials, including density, elastic modulus, and Poisson's ratio, are listed in Table 4. The sections to be modelled are those of the steel column, frame beam, bracing member, and floor.

Table 4
Material characteristics for steel frame model

Material	Density(kg/m^3)	Elastic modulus (Pa)	Poisson's ratio
Steel	7850	2.06E11	0.3
Iron	7870	2.05E11	0.28

The structural analysis of the FE model is further subdivided into analysis steps using different methods in ABAQUS. To identify the steel frame frequencies, the frequency option of the linear perturbation method is selected, and three frequency feature methods are explored: Lanczos method [29–30], subspace method, and automatic multi-level substructure method. Because extracting the frequency of steel frames is limited to low orders, the Lanczos method is used to obtain the frequencies because it demonstrates high speed and accuracy in obtaining such low-order frequencies.

The grid type, size, and partitioning significantly affect the computational complexity and accuracy of the FE modelling process. Considering the computational burden, a four-node curved thin shell is selected as the grid element, and simplified integration and hourglass control are adopted. The global grid size is determined to be 0.075. The resulting model after grid partitioning is shown in Fig. 13.

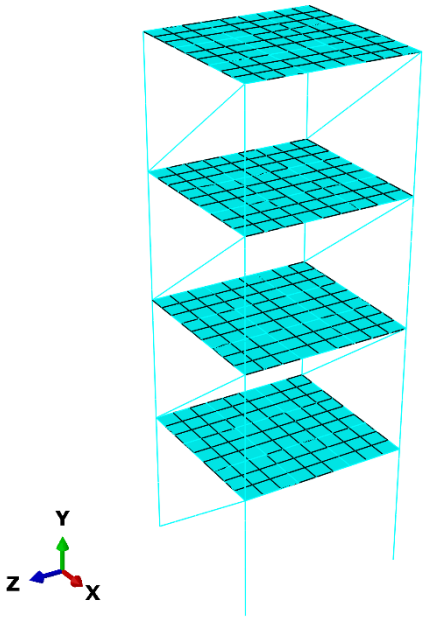

Fig. 13 Steel frame model after grid partitioning

3.2. Analysis of FE modelling results

The first, second, and third vibration modes of the steel frame are shown in Fig. 14; the black and coloured lines indicate the states of the steel frame before and after deformation, respectively. These three vibration modes conform to the structural vibration theory. The first and second vibration modes are translational in the directions of the weak (direction without bracing members) and strong (direction with bracing members) axes, respectively. The third vibration mode is torsional.

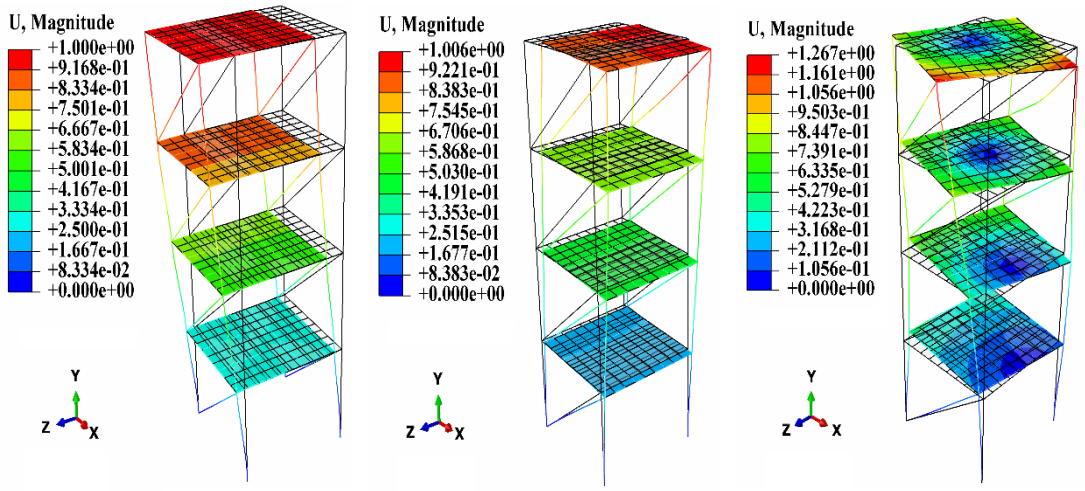

(a) First mode (b) Second mode (c) Third mode

Fig. 14 First three vibration modes of steel frame

Table 5
FE analysis steel frame frequencies from first order to fourth order under some working conditions

Working Condition	The frequencies/Hz and error							
	1st order	Error 1 (%)	2nd order	Error 2 (%)	3rd order	Error 3 (%)	4th order	Error 4 (%)
Undamaged	6.530	3.11	14.385	7.55	20.862	1.44	33.926	1.27
#1	6.528	3.08	13.349	1.38	18.863	10.53	33.920	1.63
#12	6.525	4.40	13.345	6.06	18.208	13.30	33.913	1.99
#123	6.524	7.25	13.340	6.36	18.169	13.27	33.867	3.41
#1234	6.523	15.62	13.337	13.91	18.168	5.83	33.808	3.23

A comparison of the frequencies between the FE analysis and the vibration test is summarised in Table 5. Under the no-damage condition, the errors in the results are within 8%. The error between the third-order frequency of the FE model and test results is greater than 10% under the following working conditions: (a) only bracing member ① is dismantled; (b) bracing members ① and ② are simultaneously dismantled; and (c) bracing members ① ②, and ③ are simultaneously dismantled. Under the working condition in which four bracing members (①, ②, ③, and ④) are dismantled simultaneously, the errors between the first-order and second-order frequencies of the FE model and test results are relatively large. The overall error between the FE analysis and test results shows close agreement. Therefore, using the FE model of the steel frame is reasonable.

4. Construction of damage identification model for bracing members

4.1. Overview of MobileNetV2 deep learning model

MobileNetV2 is a deeply separable CNN with linear bottlenecks and inverted residual blocks based on the MobileNetV1 model [32–36]. Deep separable convolution distinguishes convolutional channel correlation from spatial channel correlation. In contrast, conventional convolution achieves the collaborativel mapping of channel and spatial correlations [31]. Therefore, deep separable convolution compared with conventional convolution can improve network speed to a certain extent.

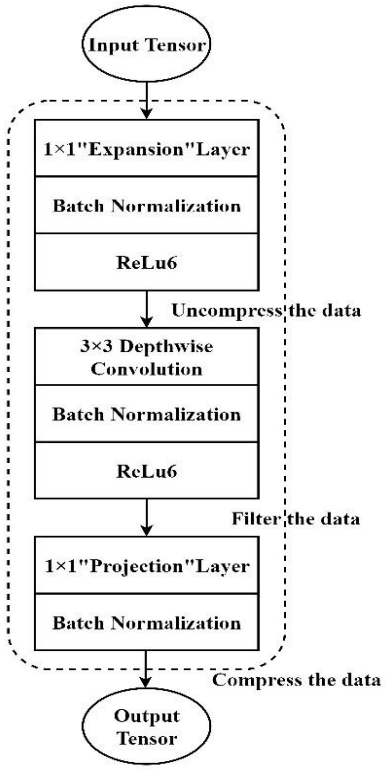

Fig. 15 Schematic of bottleneck residual block [26]

Table 6
Composition of MobileNetV2 network [26]

The size of the input	Operator
224×224×3	Convolution layer
112×112×32	Bottleneck
112×112×16	Bottleneck
56×56×24	Bottleneck
28×28×32	Bottleneck
14×14×64	Bottleneck
14×14×96	Bottleneck
7×7×160	Bottleneck
7×7×320	Convolution layer (size: 1×1)
7×7×1280	Average pooling layer (size: 7×7)
1×1×160	Convolution layer (size: 1×1)

The use of linear bottlenecks is necessary because non-linear activation functions, such as rectified linear units (ReLUs), result in the loss of image information. Furthermore, the linear bottleneck layer contains essential information, whereas the expansion layer provides a non-linear activation layer with rich information. The inversion of residual blocks involves upscaling low-dimensional image features using convolution, filtering, feature downscaling using the convolution kernel, and ReLU function to obtain the feature output. This maintains all necessary information and increases the expressiveness of the deep network.

A schematic of the bottleneck residual block is presented in Fig. 15. The composition of MobileNetV2 is listed in Table 6.

4.2. Image preprocessing

The time–frequency analysis of acceleration signals results in 69 classes of working conditions; with 24 images per class, this results in a total of 1656 images. To facilitate data labelling, the images of each class are saved in a corresponding class folder. The naming convention of image folders is consistent with that of the dismantling conditions of bracing members (Table 2).

Owing to the small number of images per class, the model cannot learn the image features well. Therefore, an image augmentation method is used to expand the dataset. Image augmentation operations commonly include image flipping, translation, clipping, and rotation [37]. Each image is uniformly resized to 224 × 224 × 3 pixels. Examples of image augmentation results are shown in Fig. 16.

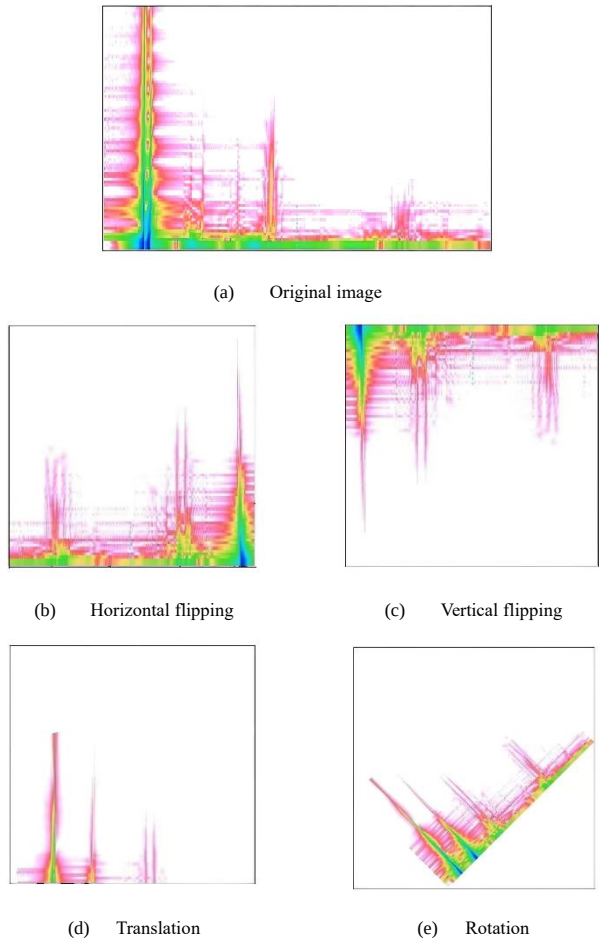

Fig. 16 Effects of image operations for data augmentation

4.3. Setup and training of MobileNetV2 model

The MobileNetV2 model is established based on Python 3.6.7 and TensorFlow 1.13. The training process was implemented on a DellG3 computer with Windows 10, Intel® Core™ i7-9750H CPU@2.60GHz, a solid-state hard drive, 16-GB RAM, and a 6-GB GPU with NVIDIA GTX1660 Ti.

The model is trained using a transfer learning approach [38]. The percentage of randomly discarded neurones in the dropout layer is set to 40%. In contrast, the number of output classes in the dense layer is set to 15, and a softmax activation function is employed. For network training and testing, 80% of the images were randomly selected to form a training set, and the remaining photos

were used for testing and evaluation. The training hyperparameters are as follows.

1. The number of training epochs is 300 with 12 iterations per epoch for 3600 iterations.

2. A small learning rate of 0.0001 is employed to enhance the learning of image features.

3. Stochastic gradient descent is used as the optimisation method because of its online learning capability and fast convergence characteristics.

4. The minimum batch size for each training iteration is 10.

An accuracy of 99.30% is achieved relative to both the training and testing sets for the prediction accuracy of MobileNetV2. The predicted outcomes of photograph selection for this project are shown in Fig. 17. The trained model for each image outputs the picture classification probabilities. As shown in Fig. 17, the probability values associated with the class predictions for the 7th and 20th images are relatively low.

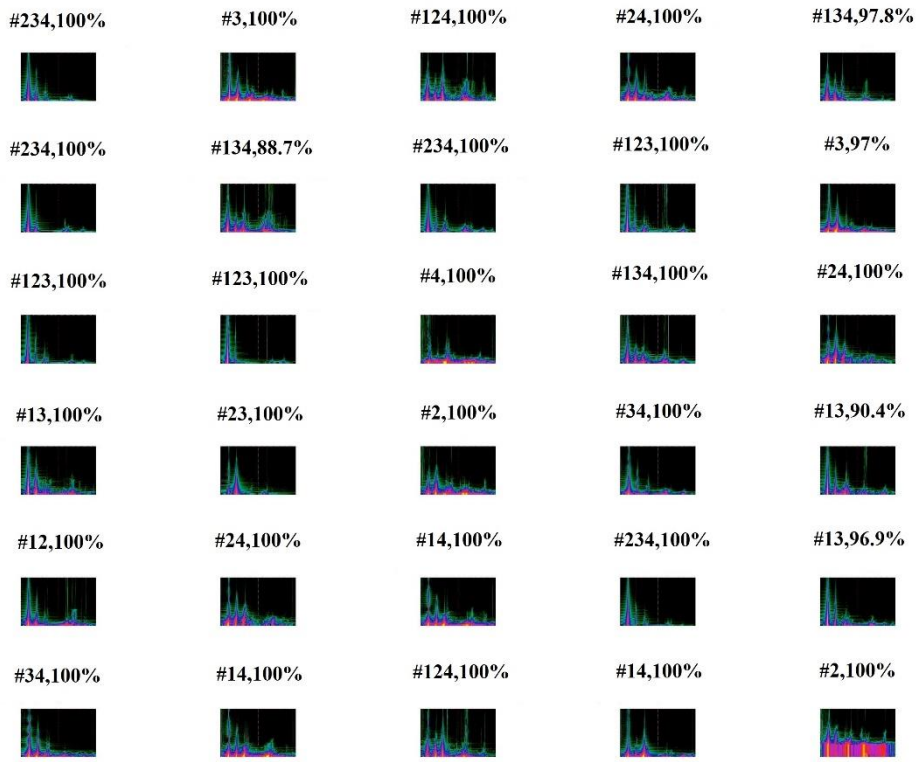

Fig. 17 Prediction results of MobileNetV2 model for some images

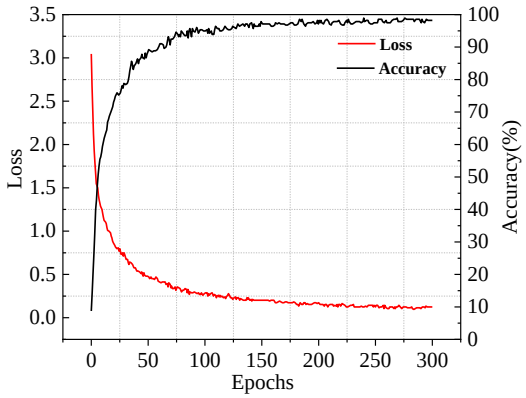

Fig. 18 Accuracy and loss curves of MobileNetV2 model for training set

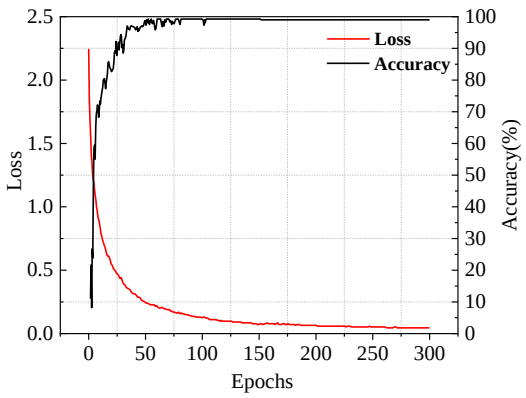

Fig. 19 Accuracy and loss curves of MobileNetV2 model for test set

The growth curves of accuracy and prediction loss over the training iterations are plotted for the training and test sets, as shown in Figs. 18 and 19, respectively. The training accuracy and loss remain stable even after 100 epochs. However, the test accuracy and loss were not smooth and did not reach relatively stable values. The final training and test loss values are 0.04557 and 0.12492, respectively.

4.4. Performance evaluation of MobileNetV2 model

Classification accuracy alone may not be a reliable indicator of model performance. For example, suppose that 90% of the data samples for a binary classification task belong to the positive class and the remaining samples belong to the negative class. Suppose a model is established to classify all data samples as positive. Although a 90% classification accuracy is considerably high, the model predicts all negative data samples as positive. Accordingly, the performance of the MobileNetV2 model is comprehensively evaluated using a confusion matrix (or contingency table) and three indicators (precision (or positive predictive value), recall (or sensitivity), and F1-score) derived from it.

The confusion matrix visually illustrates the classification results by describing the relationship between the true and predicted classes of data samples. The rows and columns of the matrix correspond to the predicted and true classes of the actual data samples, respectively.

Precision and recall are primarily used in binary classification tasks. The two evaluation indices can be derived from the four metrics of a binary classifier: number of true positives (TP), true negatives (TN), false positives (FP), and false negatives (FN). Precision and recall are computed as follows:

$$Precision = \frac{TP}{TP + FP} \tag{3}$$

$$Recall = \frac{TP}{TP + FN} \tag{4}$$

Precision and recall are not totally consistent for some classification tasks and unwarranted situations where one of the two indices is low and the other is high. Therefore, a reasonable performance analysis may not be possible using these two indices. Alternatively, the F-score index can be used to weigh and reconcile precision and recall. According to the different weights of accuracy and recall under various classification tasks, the F-score can be extended to many alternatives. Three indices are most important: F0.5-score, F1-score, and F2-score. The F1-score is used to evaluate the performance of MobileNetV2; it is calculated as follows:

$$F1 = 2 \times \frac{Precision \times Recall}{Precision + Recall} \tag{5}$$

The F1-score assigns equal importance to precision and recall and hence assigns them equal weights. For multivariate classification tasks, an F1-score can be calculated separately for each class; hence, the final F1-score can be calculated as the average of class-specific scores. This calculation can be expressed as

$$F1-score_{final} = \left(\frac{1}{n} \sum_{k=1}^{n} f1-score_k \right) \tag{6}$$

where $k = 1, 2, 3, ..., n$, and n is the number of classes.

Satisfactory improvement is introduced by the F1-score over individual precision and recall indicators; however, enhancement is limited. In general, not all F-scores incorporate inverse precision or recall. Hence, they are inferior to indicators involving all four fundamental binary classification metrics (i.e., precision, recall, inverse precision, and inverse recall). Although the F1-score suffices for the current objective in this study, it is not comparable with the Matthew correlation coefficient, which depends on the four fundamental metrics [40–41].

Owing to the several dismantling conditions of bracing members, the performance of the deep learning model is evaluated under four types of conditions or states under which one, two, three, or four bracing members are dismantled. The confusion matrices of the test set are used to evaluate model performance under each dismantling condition.

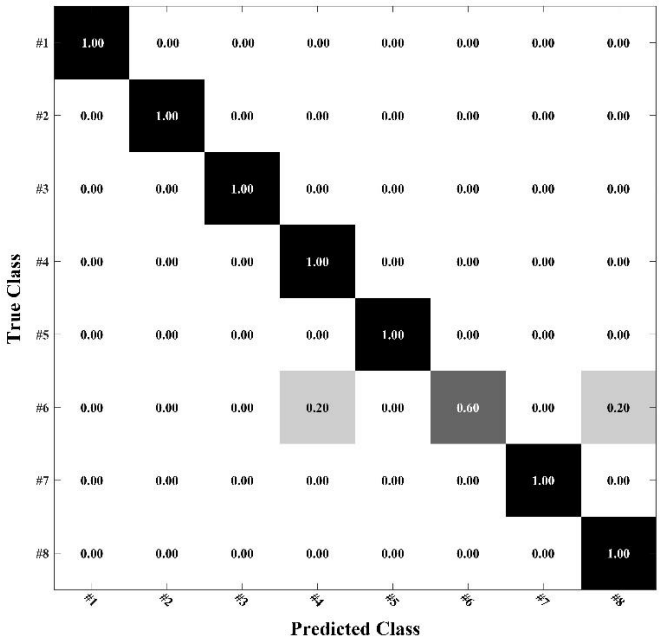

Fig. 20 Confusion matrix of MobileNetV2 model for test set when one bracing member is dismantled

4.4.1. One bracing member dismantled

The confusion matrix for the test set under the working conditions in which one bracing member is dismantled is shown in Fig. 20. The model incorrectly classifies 40% of the images in class #6 as either class #4 or class #8. The precision, recall, and F1-score of the model for the test samples of various classes are shown in Fig. 21. Because the model misclassifies the test samples of class #6 as class #4 or class #8, not all of the resulting precision and recall values reach 100% for these three classes. Incorrect classification also led to low F1-score values for the samples associated with the three classes, particularly class #6. The F1-score for the entire dataset was 0.9460, indicating good classification and prediction performance for samples collected under working conditions in which a single bracing member was dismantled.

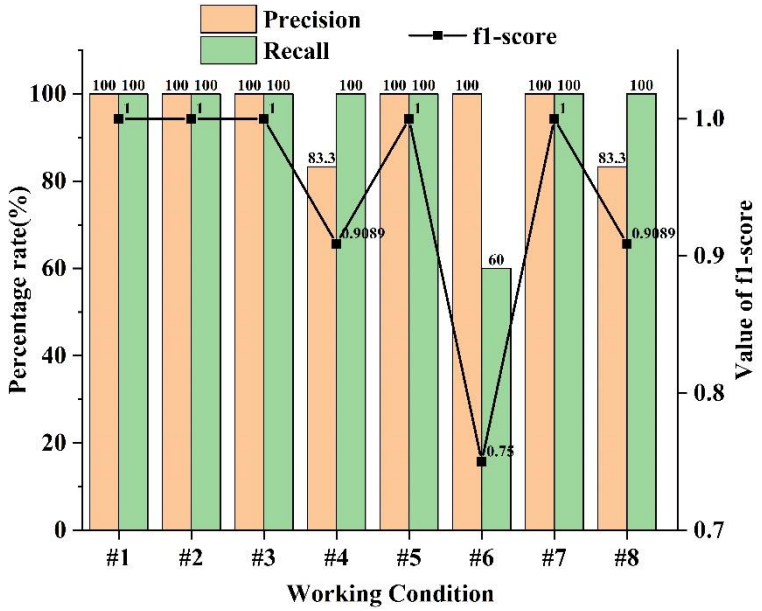

Fig. 21 Precision, recall, and F1-score of damage identification model for samples with various classes when one bracing member is dismantled

4.4.2. Two bracing members dismantled

The confusion matrix for the test set under the working conditions in which two bracing members are dismantled is shown in Fig. 22. The deep learning model correctly predicts the actual classes of all 22 sample types; however, the predictions of the model for the remaining six types are incorrect. In particular, for the samples of class #37, the model incorrectly predicted 20% of the samples, indicating that it did not adequately learn the features of class #37. The precision, recall, and F1-score of the test set are shown in Fig. 23. The models associated with classes #23, #37, and #48 showed relatively low precision or recall values, resulting in low F1-scores. The F1-score for the entire dataset is 0.9505, indicating good classification and prediction performance under the working condition in which two bracing members are dismantled.

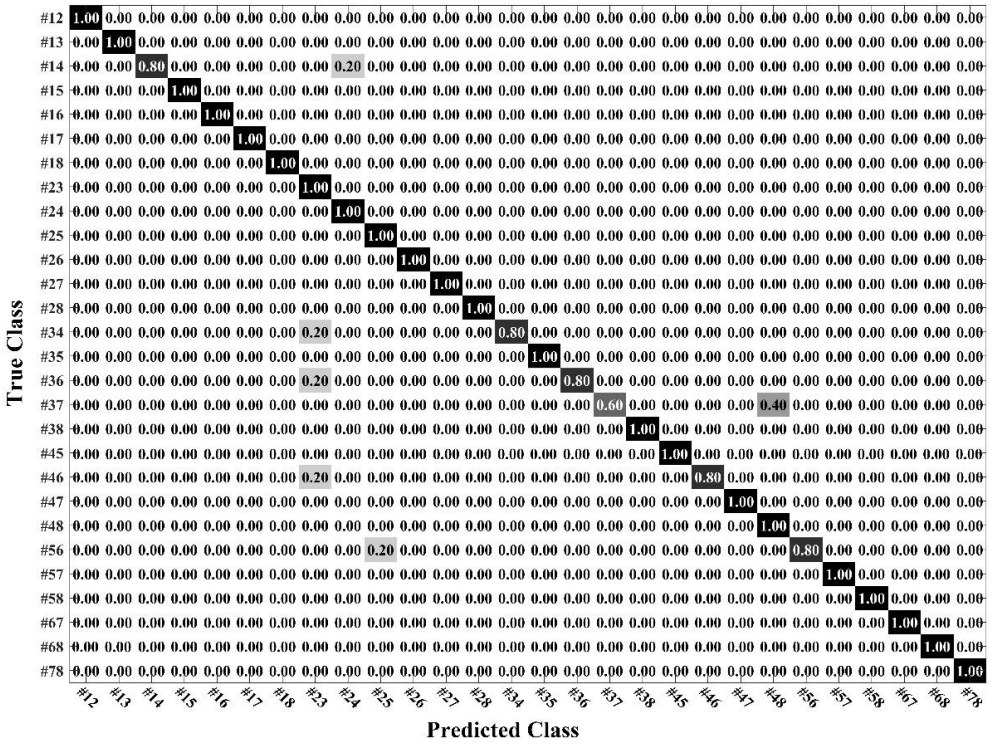

Fig. 22 Confusion matrix of MobileNetV2 model for test set where two bracing members are dismantled

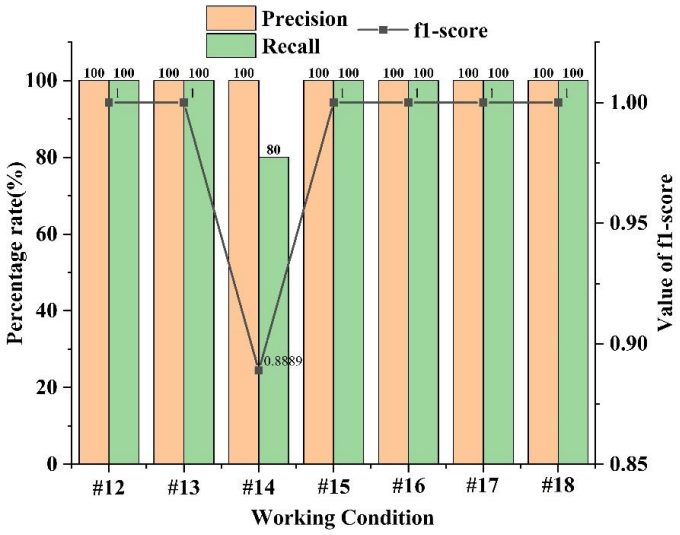

(a) Part I

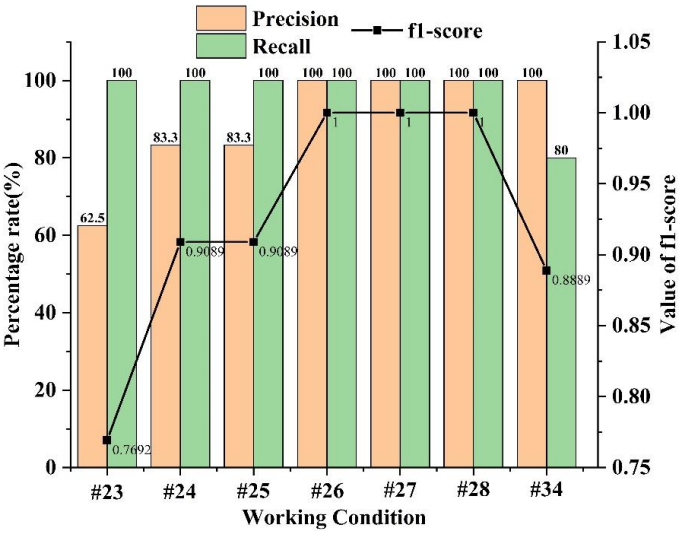

(b) Part II

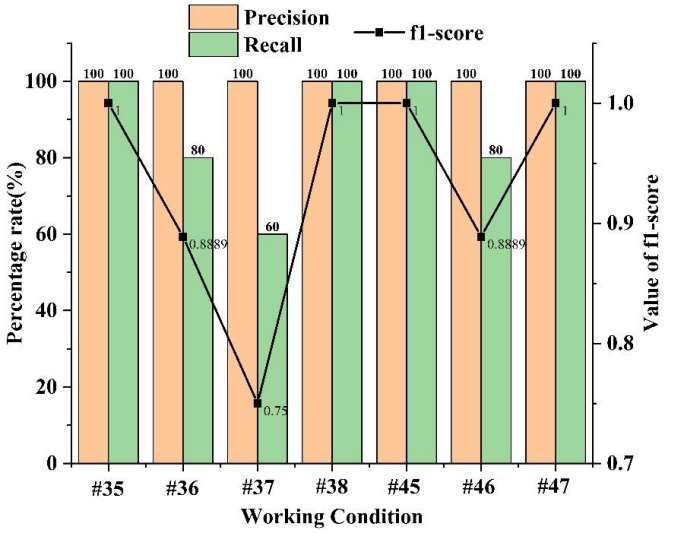

(c) Part III

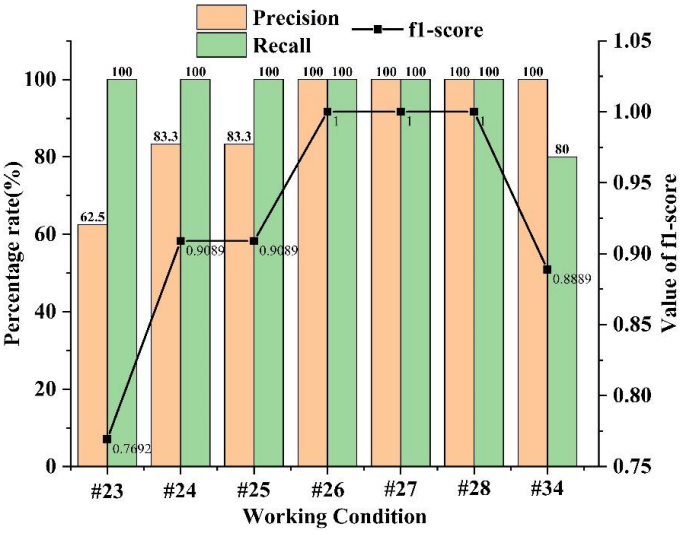

(d) Part IV

Fig. 23 Precision, recall, and F1-score of damage identification model for samples with various classes where two bracing members are dismantled

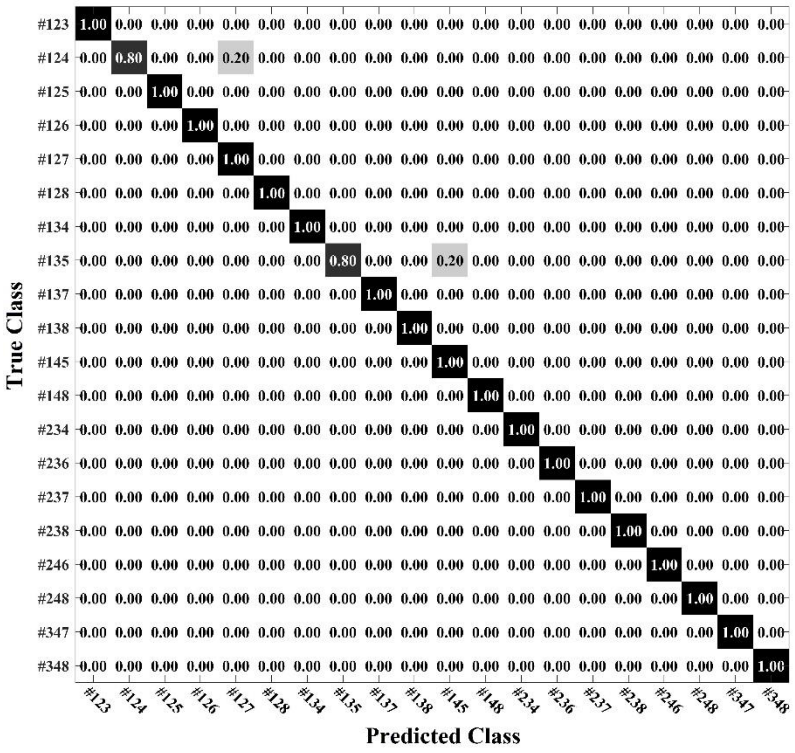

Fig. 24 Confusion matrix of MobileNetV2 model for test set where three bracing members are dismantled

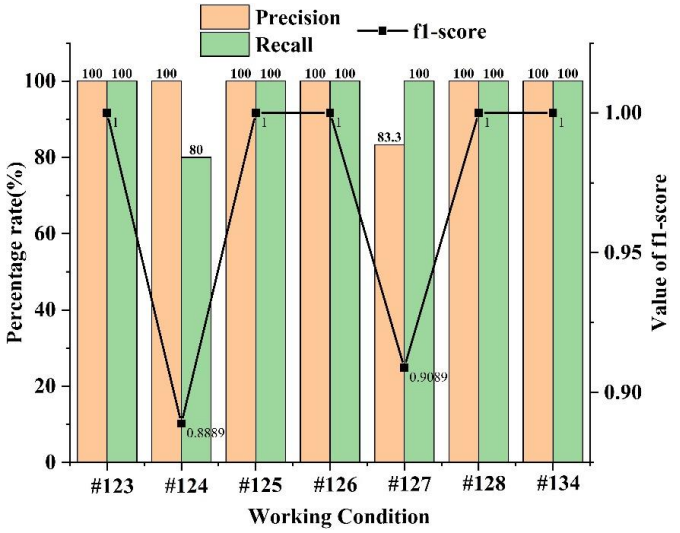

(a) Part I

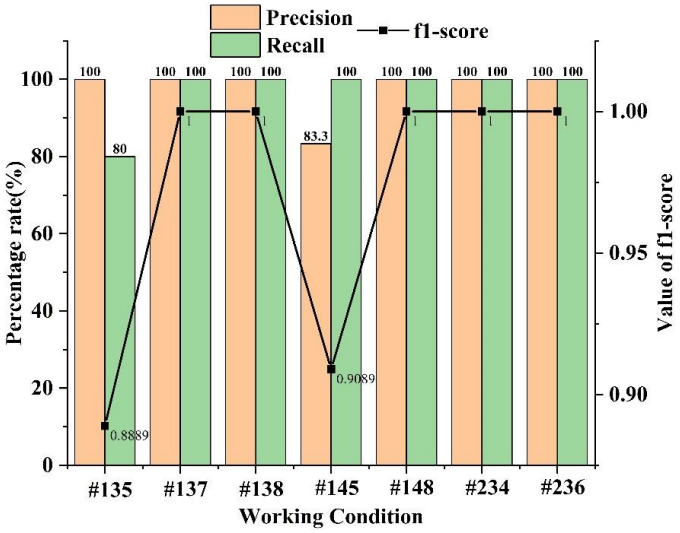

(b) Part II

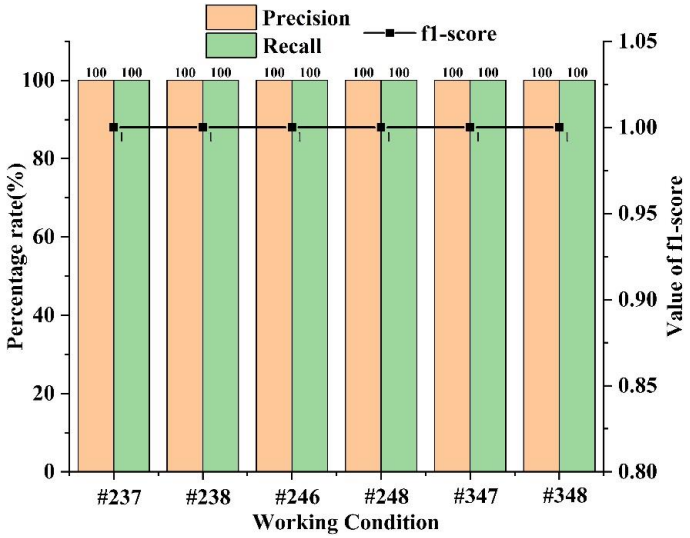

(c) Part III

Fig. 25 Precision, recall, and F1-score of damage identification model for samples with various classes where three bracing members are dismantled

4.4.3. Three bracing members dismantled

The confusion matrix of the test set under the working conditions in which the three bracing members are dismantled is shown in Fig. 24. The model made incorrect predictions for the samples of two classes: 20% of the samples of class #124 are predicted as class #127, and 20% of the samples of class #135 are expected to be those of class #145. Compared with the other classes, the model prediction performance for these two classes is relatively inadequate. The precision, recall, and F1-score of the test set are shown in Fig. 25. Because the model misclassified some samples of classes #124 and #135, not all associated precision and recall values reached 100%. The F1-score for the entire dataset was 0.9798, indicating excellent classification and prediction performance under the working condition in which three bracing members were dismantled.

4.4.4. Four bracing members dismantled

The confusion matrix of the test set under the working condition in which four bracing members are dismantled is shown in Fig. 26. The model incorrectly predicted the samples of two classes: 20% of class #1235 was predicted as class #2345 and 20% of class #2345 was predicted as class #2348. Compared with the other classes, the generalisation performance of the model for these two classes was relatively inadequate. The precision, recall, and F1-score of the test set are shown in Fig. 27. Because the model incorrectly classified some samples of classes #1235 and #2345, not all associated precision and recall values reached 100%. Misclassification also caused the model precision for class #2348 to decrease from 100% to 83.3%.

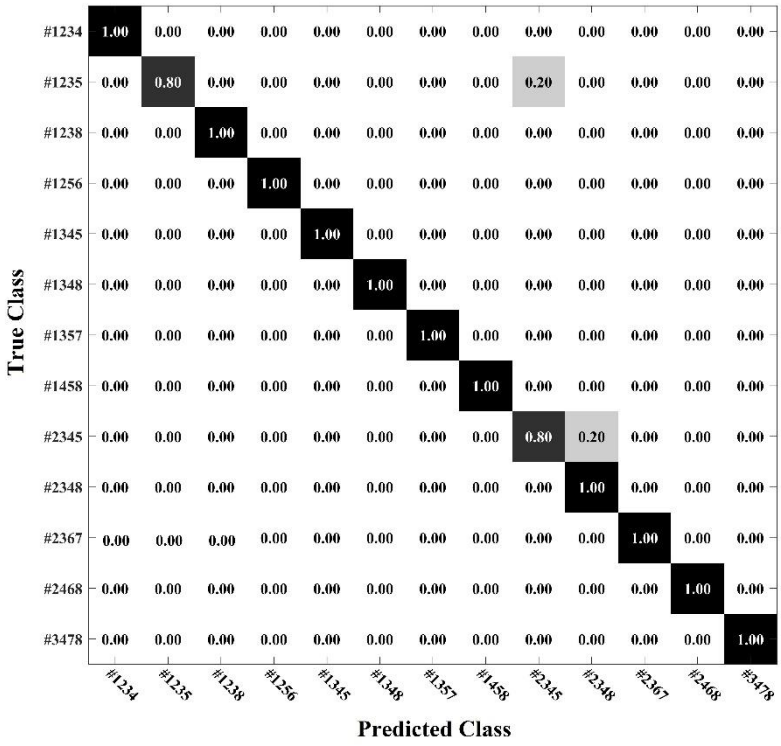

Fig. 26 Confusion matrix of MobileNetV2 model for test set where four bracing members are dismantled

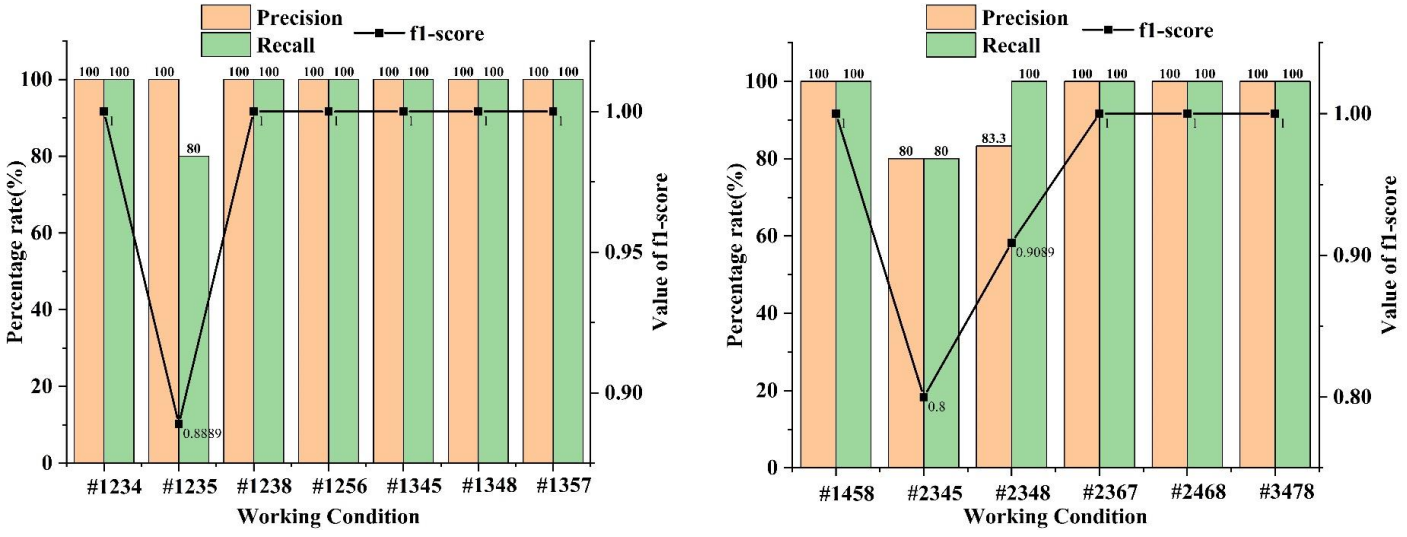

(a) Part I (b) Part II

Fig. 27 Precision, recall, and F1-score of damage identification model for samples with various classes where four bracing members are dismantled

Overall, the prediction accuracy of the trained model on the full dataset is 97.37%. Hence, the damage location of steel frame support members can be determined relatively well. However, the accuracy of the model for certain support removal conditions is low: (a) 60% when support member #6 is removed; (b) 60% when support members #3 and #7 are simultaneously removed; (c) 80% when support members #1, #2, and #4 as well as support members #1, #3, and #5 are simultaneously removed; and (d) 80% accuracy when support members #1, #2, #3, and #5 and support members #2, #3, #4, and #5 are simultaneously removed.

5. Conclusions

Time–frequency domain analysis and CNNs are used to identify lateral support failures in different parts of a steel structure. The damaged member is identified and rapidly replaced as soon as possible to ensure safety. A four-layer steel frame model with a bracing system is used to investigate a new approach for damage identification in steel structures. Specifically, a deep learning model for identifying the dismantling position of bracing members is established using transfer learning. The following conclusions are obtained based on the vibration testing and FE modelling results of the steel frame structure combined with the performance evaluation of the MobileNetV2 model.

1. The actual dynamic measurements of the model are used to obtain the modalities of the structure in each order and the modalities after the failure of various supports. These test findings are utilised to improve the FE model, enabling the acquisition of a considerable amount of more accurate training data for subsequent FE simulations.

2. Vibration tests on intact and broken support structures reveal a specific variance in the time–frequency domain. This indicates the viability of utilising CNN as a deep-learning image recognition approach.

3. The chosen MobileNetV2 network from CNN exhibits improved performance in recognising time–frequency domain images. Moreover, the trained model can discriminate distinct damage components with 99.3% accuracy.

4. As described in this research, a better approach to locate steel structure support damage is to identify damage from the structure's dynamic response. Then, the findings of the time–frequency domain analysis of the response can be inputted into the trained model.

5. The number of comparable training samples can be increased to improve damage detection. Based on the overall classification accuracy and F1-score, the MobileNetV2 model combined with time–frequency analysis provides a high degree of sensitivity and accuracy for detecting damage to support members.

Acknowledgments

The work in this paper was supported by the 2023 Yangzhou Key R&D Program (Social Development) Project Grant No SSF2023000101, Natural Science Foundation of Jiangsu Province of China under Grant No BK20200705, and the Key Technologies Research and Development Program (CN) under Grant No. 2021YFB2600600. The corresponding author expresses gratitude to the 2018 Jiangsu Provincial Government Scholarship Program (No. 228) for supporting the visit to the University of California, Los Angeles, USA.

References

[1] H. Shokravi, N. Bakhary, S.R. Koloor, M. Petru, Health Monitoring of Civil Infrastructures by Subspace System Identification Method: An Overview, Applied Sciences. 10 (8) (2020) 1-29.
[2] C. Scuro, P.F. Sciammarella, F. Lamonaca, R.S. Olivito, D.L. Carnì, Iot for Structural Health Monitoring, IEEE Instrumentation and Measurement Magazine.
21 (6) (2018) 4-9 and 14.
[3] K. Geissler, N. Steffens, R. Stein, Basics of the safety-equivalent assessment of
bridges with structural health monitoring, STAHLBAU. 88 (4) (2019) 338-353.
[4] S.O. Sajedi, X. Liang, Uncertainty - assisted deep vision structural health monitoring, Computer-Aided Civil and Infrastructure Engineering. 36 (2) (2021) 126-142.
[5] Y. Kankanamge, Y. Hu, X. Shao, Application of wavelet transform in structural health monitoring, Earthquake Engineering and Engineering Vibration. 19 (02) (2020) 515-532.
[6] O. Yazdanpanah, B. Mohebi, M. Yakhchalian, Seismic damage assessment using improved wavelet-based damage-sensitive features, Journal of Building Engineering. 33 (2020) 101311.
[7] B. Mohebi, O. Yazdanpanah, F. Kazemi, A. Formisano, Seismic damage diagnosis in adjacent steel and RC MRFs considering pounding effects through improved wavelet-based damage-sensitive feature, Journal of Building Engineering. 33(2020) 101847.
[8] T. Tam, D. Dinh, J. Lee, T. Nguyen, An effective deep feedforward neural networks (DFNN) method for damage identification of truss structures using noisy incomplete modal data, Journal of Building Engineering. 30 (2020) 101244.
[9] Y. Xin, J. Li, H. Hao, Damage Detection in Initially Non-linear Structures based on Variational Mode Decomposition, International Journal of Structural Stability & Dynamics. 20 (10) (2020) 2042009.
[10] J. Liu, Z. Lu, M. Yu, Damage identification of non-classically damped shear building by sensitivity analysis of complex modal parameter, Journal of Sound and Vibration. 438 (2019) 457-475.
[11] J. Han, P. Zheng, H. Wang, Structural modal parameter identification and damage diagnosis based on Hilbert-Huang transform, Earthquake Engineering and Engineering Vibration. 13 (1) (2014) 101-111.
[12] A. Paral, D. Roy, A.K. Samanta, A deep learning-based approach for condition assessment of semi-rigid joint of steel frame, Journal of Building Engineering. 34, 2021, 101946.
[13] C. Pathirage, J. Li, L. Li, H. Hao, W. Liu, R. Wang, Development and application of a deep learning-based sparse autoencoder framework for structural damage identification, Structural Health Monitoring. 18 (1) (2019) 103-122.
[14] C. Pathirage, J. Li, L. Li, H. Hao, W. Liu, R. Wang, P.H. Ni, Structural damage identification based on autoencoder neural networks and deep learning, Engineering Structures. 172 (2018) 13-28.
[15] S. Hakim, H.A. Razak, Frequency Response Function-based Structural Damage Identification using Artificial Neural Networks-A review, Research Journal of Applied Sciences Engineering & Technology. 7 (9) (2014) 1750-1764.
[16] S. Hakim, H.A. Razak, S.A. Ravanfar, Ensemble neural networks for structural damage identification using modal data, International Journal of Damage Mechanics. 25 (3) (2016) 400-430.
[17] P. Seventekidis, D. Giagopoulos, A. Arailopoulos, O. Markogiannaki, Structural Health Monitoring using deep learning with optimal FE model generated data, Mechanical Systems and Signal Processing. 145 (2020) 106972.
[18] T. Liu, H. Xu, M. Ragulskis, M. Cao, W. Ostachowicz, A Data-Driven Damage Identification Framework Based on Transmissibility Function Datasets and One- Dimensional Convolutional Neural Networks: Verification on a Structural Health Monitoring Benchmark Structure, Sensors. 20 (4) (2020) 1059.
[19] E. Figueiredo, I. Moldovan, A. Santos, P. Campos, C.W. Costa, Finite Element-Based Machine-Learning Approach to Detect Damage in Bridges under Operational and Environmental Variations, Journal of Bridge Engineering. 24 (7) (2019) 1432.
[20] Nadith P, Li J, Ling L, et al. Structural damage identification based on autoencoder neural networks and deep learning. Engineering Structures, 2018, 172: 13-28.
[21] Gordan M, Ismail Z, Razak H A, et al. Data mining-based damage identification of a slab-on-girder bridge using inverse analysis. Measurement, 2019, 151.
[22] Ali R, Cha Y J. Subsurface damage detection of a steel bridge using deep learning and uncooled micro-bolometer. Construction and Building Materials, 2019, 226(30): 376-387.
[23] Kourehli S S, Ghadimi R. Vibration analysis and identification of breathing cracks in beams subjected to single or multiple moving mass using online sequential extreme learning machine. Inverse Problems in Science and Engineering. 2019, 27(08): 1057-1080.
[24] Teng Z Q, Teng S, Zhang J Q, et al. Structural Damage Detection Based on Real-Time Vibration Signal and Convolutional Neural Network. Applied Sciences, 2020, 10(14): 4720.
[25] Luke, H. D. The origins of the sampling theorem. IEEE Communications Magazine, 1999, 37(4), 106-108.
[26] Jerri, A. J.. The Shannon sampling theorem—Its various extensions and applications: A tutorial review. Proceedings of the IEEE, 1977, 65(11), 1565-1596.
[27] Song, Z., Liu, B., Pang, Y., Hou, C., & Li, X.. An improved Nyquist–Shannon irregular sampling theorem from local averages. IEEE transactions on information theory, 2012, 58(9), 6093-6100.
[28] Vaidyanathan, P. P.. Generalizations of the sampling theorem: Seven decades after Nyquist. IEEE Transactions on Circuits and Systems I: Fundamental Theory and Applications, 2001, 48(9), 1094-1109.
[29] Paige, C. C.. Computational variants of the Lanczos method for the eigenproblem. IMA Journal of Applied Mathematics, 1971, 10(3), 373-381.
[30] Golub, G. H., & Underwood, R.. The block Lanczos method for computing eigenvalues. In Mathematical software. 1977, 361-377. Academic Press.
[31] Chollet F. Xception: Deep learning with depthwise separable convolutions. Proceedings of the IEEE conference on computer vision and pattern recognition. 2017: 1251-1258..
[32] Sandler M, Howard A, Zhu M, et al. Mobilenetv2: Inverted residuals and linear bottlenecks。Proceedings of the IEEE conference on computer vision and pattern recognition. 2018: 4510-4520.
[33] Nguyen H. A lightweight and efficient deep convolutional neural network based on depthwise dilated separable convolution, Journal of Theoretical and Applied Information Technology. 98 (15) (2020) 2937-2947.
[34] Ananthanarayana T, Ptucha R, Kelly S C. Deep learning based fruit freshness classification and detection with CMOS image sensors and edge processors. Electronic Imaging, 2020, 2020(12): 172-1-172-7.
[35] Nguyen H. Fast object detection framework based on mobilenetv2 architecture and enhanced feature pyramid. J. Theor. Appl. Inf. Technol, 2020, 98(05). 812-824.
[36] Buiu C, Dănăilă V R, Răduţă C N. MobileNetV2 ensemble for cervical precancerous lesions classification. Processes, 2020, 8(5): 595-624.
[37] Li, W., Chen, C., Zhang, M., Li, H., & Du, Q.. Data augmentation for hyperspectral image classification with deep CNNs. IEEE Geoscience and Remote Sensing Letters, 2018, 16(4), 593-597.
[38] Torrey, L., & Shavlik, J.. Transfer learning. In Handbook of research on machine learning applications and trends: algorithms, methods, and techniques. 2010, 242-264. IGI global.